Top Catal (2013) 56:1184–1191
DOI 10.1007/s11244-013-0084-4

ORIGINAL PAPER

Nickel Nanoparticles Stabilized by Luminescent Labile Ligands

Meital Shviro · Meital Eckshtain-Levi · Laurent Benisvy · David Zitoun

Published online: 26 June 2013

Abstract Nickel nanoparticles (NPs) have been synthesized through the microwave decomposition of $Ni(\eta^4\text{-}C_8H_{12})_2$ in the presence of *o*,*p*-*t*Bu-protected salicylamide ligands with one (LH1) or two arms (LH2). The nanoparticle colloidal dispersions are stable in ethanol. The presence of ligand on Ni surface is confirmed by the UV–Vis spectroscopy, fluorescence and mass spectrometry. Furthermore, the surface ligands can easily react with metal cations to form complexes as demonstrated from the luminescence of Tb(III) complexes. Depending on the ligand, the complexes are washed away from Ni NP surface or grafted on the surface. These hybrid structures are versatile building blocks, easily dispersible in polar solvents, luminescent and magnetic.

Keywords Nickel · Nanocrystals · Shape control · Magnetism · Luminescence

1 Introduction

Supported nickel nanoparticles (NPs) have been used as catalysts for several classes of reactions: hydrolysis, hydrogenation, C–H activation or cross-coupling, without focusing on electrocatalytic activity in fuel cells [1, 2]. For instance, aminoborane hydrolysis is efficiently catalyzed by Ni NPs [3]. Ni(0) in the forms of NPs catalyze hydrogen transfer reactions [4]. In coupling reactions, Ni nanoparticles can replace platinum group metals like Pd in the Suzuki coupling reactions [5]. While Pd NPs surface chemistry has been extensively investigated [6, 7], a similar research on Ni NPs surface should bring a significant edge to the more affordable Ni metal, and complete the recent study of the catalytic activity of size selected colloidal Ni NPs [3]. Furthermore, functional ligands and complexes on the surface of active nanocatalysts represent a step further at the frontier between homogeneous and heterogeneous catalysis [8].

Ni NPs syntheses have been performed using strongly binding ligands like bulky phosphine using $Ni(acac)_2$ as precursor [5]. Such a ligand shell is detrimental to the activity and should be removed by thermal desorption. Milder reaction conditions avoid such a post-synthetic process using long chain amines and ammonia borane chemical reduction of $Ni(acac)_2$ [3]. Nevertheless, the synthesis still process through acetylacetonate and hydrophobic amine ligands (oleylamine).

On the other hand, the use of organometallic precursors has proved to be very efficient in order to synthesize metallic NPs in mild conditions with a clean metallic surface. Organometallic precursor like Ni(1,5-cyclooctadiene)$_2$ ($[Ni(COD)_2]$ or $[Ni(\eta^4\text{-}C_8H_{12})_2]$) has successfully yielded Ni NPs with a broad range of sizes, stabilized with a polymer (PVP or PEO) [9, 10], imidazolium ionic liquid [11], or anthranilic acid [12]. In all cases, nearly spherical NPs could be stabilized in THF or ionic liquid. In another study, hydrogen assisted decomposition of $[Ni(\eta^4\text{-}C_8H_{12})_2]$ yielded a mixture of Ni faceted NPs and nanorods in presence of an excess of hexadecylamine ligand [13].

Meital Shviro and Meital Eckshtain-Levi equally contributed to this study.

M. Shviro · M. Eckshtain-Levi · L. Benisvy (✉) · D. Zitoun (✉)
Department of Chemistry, Bar Ilan Institute of Nanotechnology and Advanced Materials, Bar Ilan University, 52900 Ramat Gan, Israel
e-mail: Benisvl@mail.biu.ac.il

D. Zitoun
e-mail: david.zitoun@biu.ac.il

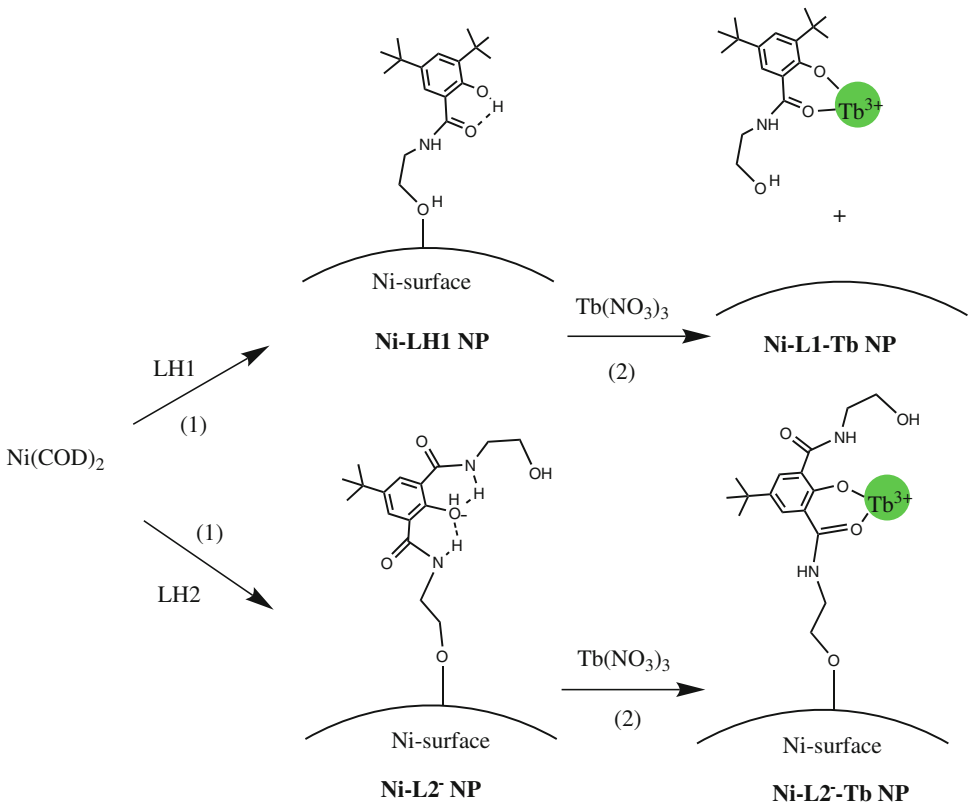

Fig. 1 Schema of the Ni NPs synthesis *(1)* and proposed coordination mode of the ligands and subsequent terbium-LH complex formation *(2)*

Thermal decomposition of $(Ni(\eta^4\text{-}C_8H_{12})_2]$ led to Ni nanowires on various substrates [14] while microwave assisted decomposition yielded pyramidal and cubic Ni NPs [15].

Interestingly, no fluorescent probe has been attached at the surface of Ni NPs synthesized from organometallic decomposition to follow the sorption mechanism and aggregation state.

Herein we have used phenol-amide (ortho-salicylamide) and phenol-diamide (2-hydroxyisophtalamide) pro-ligands possessing either one or two alcohol pendant arms, respectively (Fig. 1). These pro-ligands are of interest for several reasons: (a) they coordinate divalent and trivalent transition metals or lanthanide(III) ions in a monoanionic {*OO*}-bidentate chelating mode (acac-type) involving the coordination of both the *O*-phenolate and *O*-carbonyl donor atoms [16, 17]. (b) They are known to exhibit a short-life time (<5 ns) broad blue emission at around 450 nm when excited in the far-UV region (300–400 nm) [15]. (c) They are efficient sensitizers to the green Tb(III) and red Eu(III) emission [15]. In these compounds, the spin and parity forbidden *f–f* emission of the Ln(III) ion is rendered possible by efficient population of the emitting 4*f* excited states achieved through antenna effect, via intramolecular energy transfer from the ligand excited state to a Ln *f*-excited state. Thus the resulting sensitized Ln(III) complexes display characteristic line-like and long-life time (ca. ms) emission. (d) The pro-ligand LH1 is redox-active in its deprotonated phenolate and is readily oxidized at relatively low potential (ca. −0.1 V vs. Fc^+/Fc) yielding a persistent phenoxyl radical [18].

Clearly, the coordination, the luminescence, the Ln-sensitization, and the redox properties of these pro-ligands make them valuable candidate for the preparation of multifunctional nanomaterials. On the one hand the luminescence properties of these pro-ligands should allow to probe their adsorption on NP. On the other hand, the redox properties may assist/enhance the catalytic activity of the grafted NPs.

Herein, we report, using these pro-ligands, that discrete well-defined Ni nanostructures as colloidal dispersion, can be prepared by microwave assisted thermal decomposition of $Ni(\eta^4\text{-}C_8H_{12})_2$. Our results indicate that the NPs are stabilized by both ligands adsorbed on the surface, as correlated by their luminescent properties. Moreover, in the presence of Tb(III) ions, sensitized Tb-complexes are formed either on the surface of the NPs (with LH2) or in solution leaving surface-free Ni NPs (with LH1).

2 Results

The pro-ligands, LH1 and LH2 (Fig. 1), have been synthesized and characterized according to the reported

procedure [19]. Both ligands were reacted with the organometallic Ni precursor ($Ni(COD)_2$) in a microwave reaction under nitrogen at 100 °C for 5 min. During the process, the $Ni(COD)_2$ is thermally decomposed and 1,5-cyclooctadiene is released as a byproduct; and a black colloidal dispersion of Ni(0) is obtained. Whilst the role of the pro-ligands is at this stage unclear, the reaction kinetics does not seem to be altered by their presence. The colloids were dispersed in ethanol and centrifuged, this procedure was repeated three times to remove excess of free ligand. The colloids disperse easily in polar solvents such as THF or ethanol, resulting in stable colloidal dispersions for both LH1 and LH2 ligands. In contrast, when the reaction was performed in the absence of the pro-ligands, formation of large aggregates of Ni was observed.

Thus, LH1 and LH2 are stabilizing Ni NPs in polar solvents and transmission electron microscopy (TEM) has been used to measure particles size and aggregation state (Fig. 2). As shown in Fig. 2a, two types of Ni-LH1 NPs are formed with trigonal or rodlike shapes, with sizes ranging from 20 to 50 nm. Within this size range, Ni already displays a ferromagnetic behavior, making these NPs easily extractable in the magnetic field of a small permanent magnet. Selected area electron diffraction shows the presence of metallic Ni only, without noticeable traces of NiO. The NPs crystallize in the face-centered cubic (FCC) phase with lattice parameters corresponding to bulk Ni (*Fm*-3*m*, a = 3.52 Å) (JCPDS-04-0850).

In the case of Ni-LH2 colloidal dispersion, well dispersed nanoparticles are observed on the TEM grid; the inorganic particle cores possess a mean diameter of $D = 5 \pm 1$ nm. For this size, Ni NPs are still in the superparamagnetic regime and magnetic dipole interactions are too low to favor aggregation. The Ni-LH2 NPs crystallize in the FCC phase with lattice parameters corresponding to bulk Ni (*Fm*-3*m*, a = 3.52 Å) (JCPDS-04-0850) as shown from the X-ray diffractogram (Fig. 3). X-ray diffraction does not show the expected ratio between the [111] and the [200] reflections, which has already been observed in colloidal systems [5].

The presence of the ligand on the surface of these NPs is revealed by mass spectrometry and UV–Vis absorption and emission measurements, as well as by their reactivity with Tb(III) ions. Mass spectrometry measurements confirm the

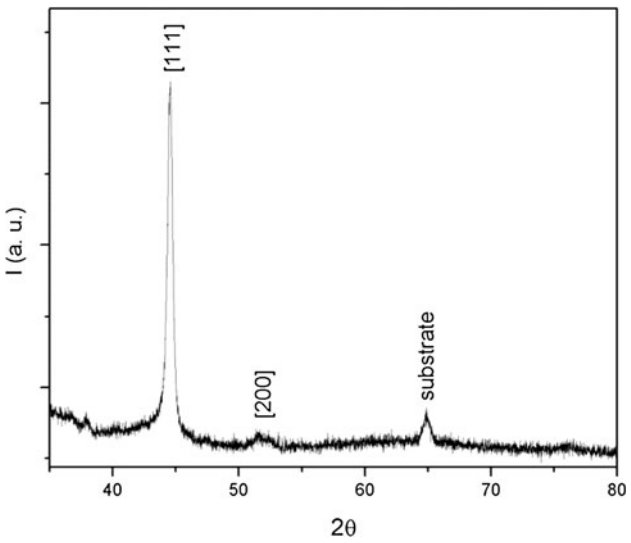

Fig. 3 X-ray diffractogram of a thin film of Ni-LH1 deposited on glass

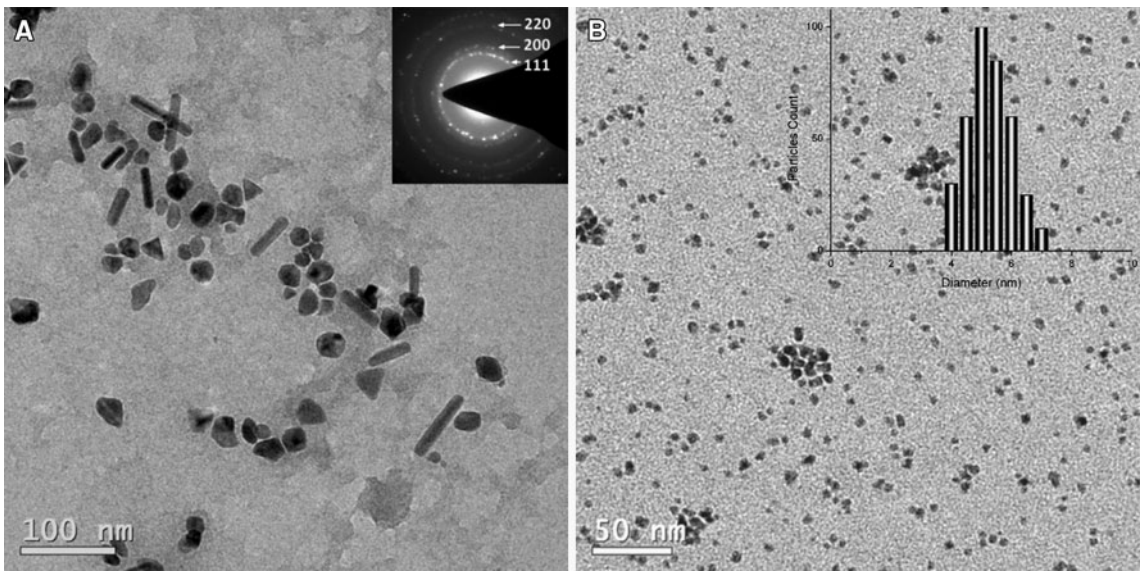

Fig. 2 Transmission electron microscopy of Ni NPs dispersed in ethanol with ligand LH1 (*inset* SAED of the corresponding area) (**a**) and LH2 (*inset* size histogram) (**b**)

presence of ligand LH1 and LH2 on the Ni surface; $[M–H]^-$ peak at *m/z* 292 and 323 (LH1 and LH2 respectively) are obtained for both the free pro-ligand and the ligand attached to the Ni surface.

Excitation and emission fluorescence (Fig. 4), UV–Vis spectroscopy (Fig. 5) have been collected for the free ligands, their mono-anionic phenolate form and their corresponding NPs dispersion in ethanol. All measurements have been arbitrary normalized ought to the difficulty to accurately measured ε values for NPs dispersions and the wavelengths for each peaks are presented in Table 1.

As expected for salicylamide and 2-hydroxyisophatlamide compounds [17], both LH1 and LH2 exhibit a broad blue emission band at 456 and 443 nm, respectively. The excitation spectrum displays a sharp band at 350 nm for LH1 and at 370 nm for LH2. For both compounds, upon deprotonation, a blue shift of ca. 20 nm of the emission band is observed (from 456 to 436 nm for L1 and 443 to 420 nm for L2); while the excitation spectra exhibit three peaks (266, 293, 366 nm for $L1^-$ and 270, 310, 387 nm for $L2^-$) instead of one peak for the protonated parent compounds. These spectroscopic features serve as a benchmark to understand the protonation state as well as the mode of coordination of these ligands to the nickel NP surface. First, it is observed that both the Ni-LH1 and Ni-LH2 dispersions in EtOH (after careful washing of the free

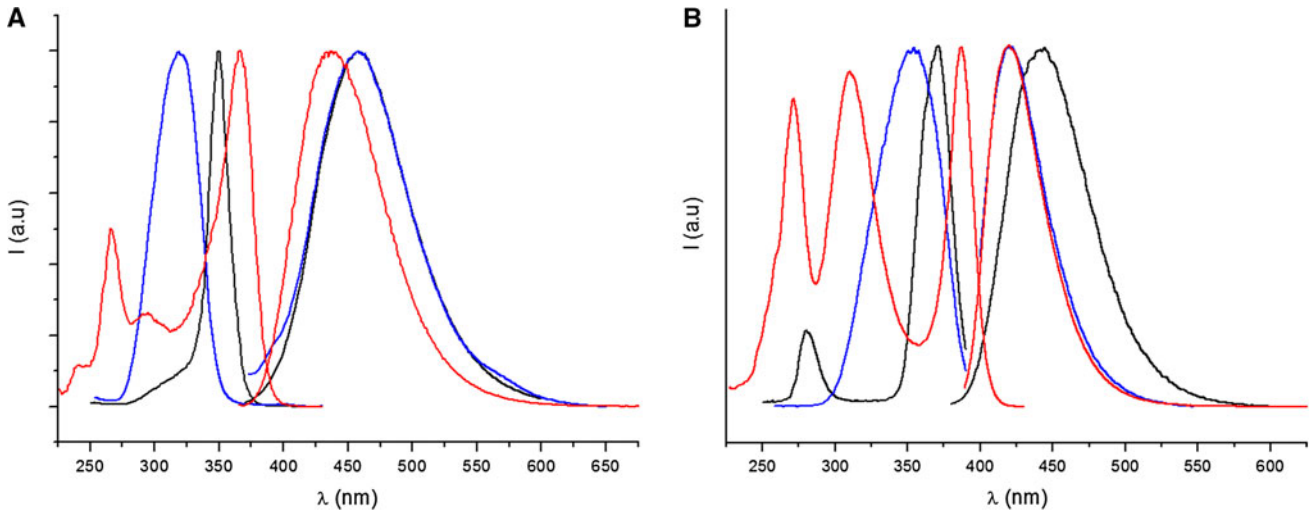

Fig. 4 Excitation ($\lambda_{em} = 450$ nm) and emission ($\lambda_{ex} = 320$ nm) spectra of LH1 (*black line*), $L1^-$ (*red line*) and Ni-LH1 colloidal dispersion (*blue line*) in EtOH (**a**); Excitation ($\lambda_{em} = 420$ nm) and emission ($\lambda_{ex} = 350$ nm) spectrum of LH2 (*black line*), $L2^-$ (*red line*), and Ni-LH2 colloidal dispersion (*blue line*) in EtOH (**b**)

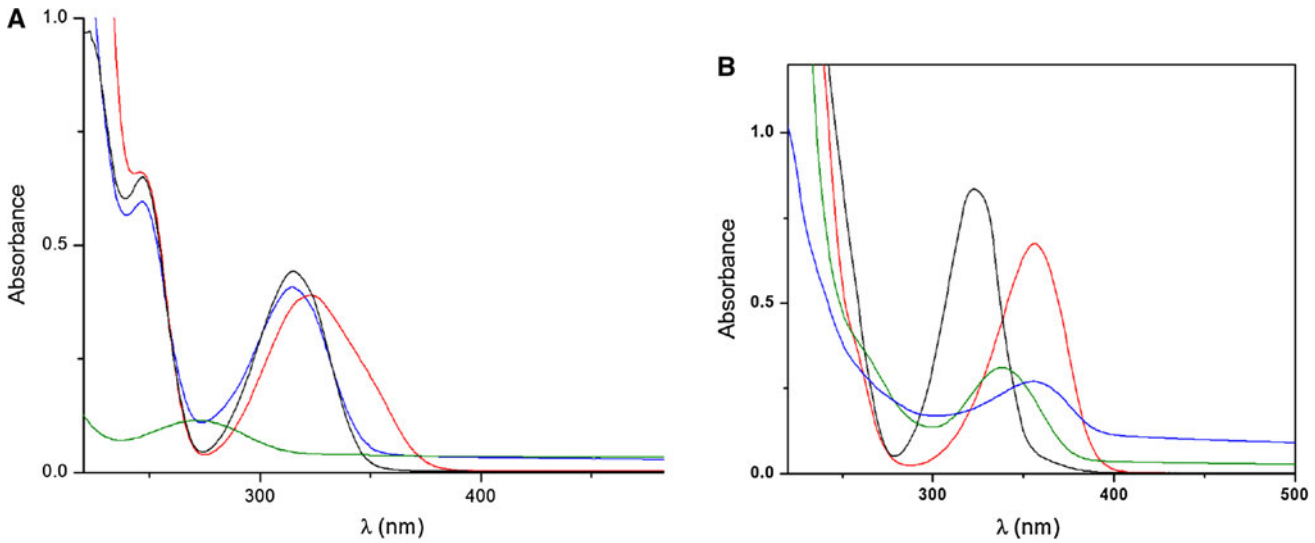

Fig. 5 UV–Vis spectra of LH1 (*black line*), $L1^-$ (*red line*), colloidal dispersions of Ni-LH1 (*blue line*) and Ni-LH1-Tb (*green line*) in EtOH (**a**); LH2 (*black line*), $L2^-$ (*red line*), colloidal dispersions of Ni-LH2 (*blue line*) and Ni-L2-Tb (*green line*) in EtOH (**b**)

Table 1 Spectroscopic data from fluorescence and UV–Vis spectroscopy measurements

	Excitation (nm)	Emission (nm)	UV–Vis (nm)
LH1	350	456	315
$L1^-$	266, 293, 366	436	320
Ni-LH1	319	456	315
Ni-LH1-Tb	275	None	275
Ni-LH1-Tb supernatant	329	414, 490, 545, 585, 623, 702	315
LH2	280, 370	443	322
$L2^-$	270, 310, 387	420	356
Ni-LH2	354	420	356
Ni-L2-Tb	333	414, 490, 545, 585, 623, 702	337

ligands) display a blue emission at 456 and 420 nm respectively, clearly indicating that the luminescent properties of the ligands are retained when bound to the NPs, and no quenching is observed. Since the fluorescence is associated to the phenol-amide unit, this may imply that the attachment to the NP surface does not involve the phenol group but rather occurs via the *O*-alcohol arm (Fig. 1). For Ni-LH1, the emission observed at 456 nm is identical to that of LH1; however, the excitation spectrum shows a peak at 319 nm, blue shifted compared to the free ligand ($\lambda_{max} = 350$ nm). These observations suggest that the ligand LH1 adsorbs on the Ni-surface in its protonated form. In contrast, the emission peak of Ni-LH2 is found at lower wavelength (420 nm) than that of LH2 (443 nm) and rather resembles the emission of the deprotonated $L2^-$ (420 nm). These observations may suggest that LH2 is adsorbed on the surface in its deprotonated form.

The UV–Vis spectroscopy confirms that LH1 ligand adsorbs to Ni in its protonated state, while deprotonated $L2^-$ chemisorbs Ni. Indeed, the UV–Vis spectrum of dispersed Ni-LH2 matches that of the anion $L2^-$ with a band at 356 nm (Fig. 5). However, the spectrum of dispersed Ni-LH1 shows a band at lower wavelength (322 nm) characteristic of the protonated LH1 ligand (Fig. 5).

Since these types of ligands are known to coordinate Tb(III) ions through a *O*,*O*-chelation, and efficiently sensitize the Ln(III) ion green emission [17], we have conducted further reactions on the surface of the NPs with the addition of Tb(III) ions. After lanthanide addition, the colloids have been thorough fully washed with ethanol to remove the excess of free Tb(III) ions, and the luminescence properties of both the colloidal dispersion and the supernatant have been measured (Fig. 6). Interestingly, In the case of Ni-LH1, upon excitation at 330 nm, the characteristic six line-like Tb(III) emissions ($\lambda_{max} = 414$; 490; 545; 585; 623; 702 nm) are observed only for the supernatant solution but not for the colloidal dispersion (Fig. 6a, b). Moreover, the resulting colloidal dispersion presents neither emission at 450 nm nor absorption in the 300–400 nm region of the excitation spectrum, clearly indicating that the ligands are no longer present at the surface of the NPs. Thus, upon reaction with Tb(III) ions, the ligands LH1 form Tb-complexes (as confirmed by the sensitization of the Tb(III) green emission) which are getting detached from the NPs surface, leaving ligand-free Ni NPs. On the contrary, in the case of Ni-LH2, the typical Tb(III) emissions are observed for colloidal dispersion but not for the supernatant (Fig. 6). Thus, in this case, Tb(III) complexes are formed on the surface by the coordination of the adsorbed ligands to the Tb(III) ions.

These results are confirmed by UV–Vis spectra (Fig. 5) of the washed and redispersed NPs after Tb-complexation reaction, clearly showing the ligand removal for Ni-LH1. In contrast, a band at 337 nm is observed for Ni-L2-Tb blue shifted from that of the parent Ni-LH2 by 19 nm. This clearly indicates that the surface ligand is coordinated to the Tb(III) ion. Solution studies show that the reactions of

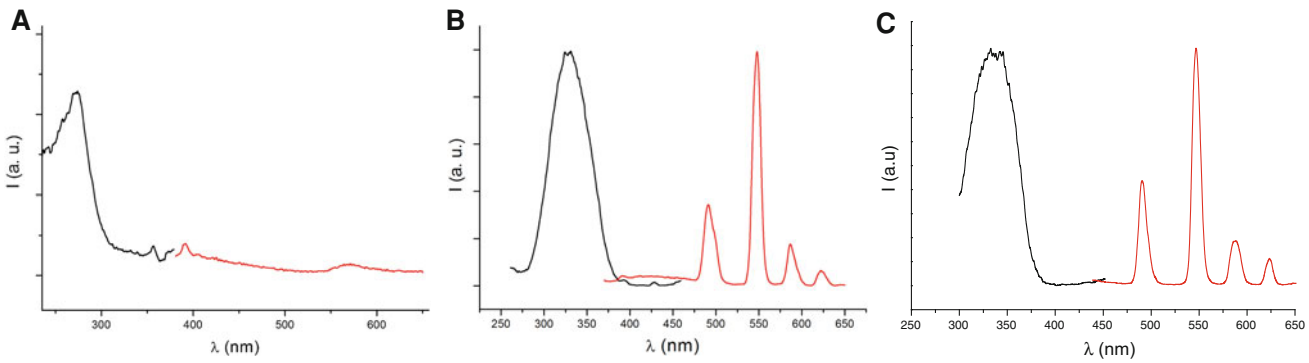

Fig. 6 Excitation ($\lambda_{em} = 550$ nm) and emission ($\lambda_{ex} = 350$ nm) spectrum after Tb(III) complexation (excitation: *black* and emission: *red*); Ni- LH1 redispersed in ethanol after washing (**a**); supernatant of Tb/LH1 (**b**); Ni- LH2 redispersed in ethanol after washing (**c**)

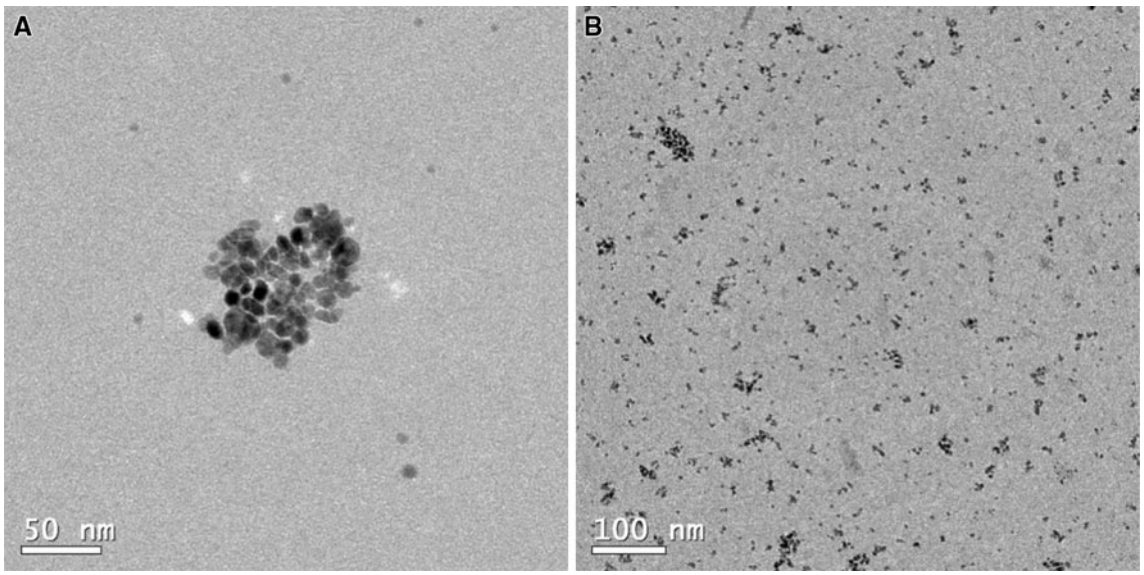

Fig. 7 Transmission electron microscopy of Ni NPs dispersed in ethanol after Tb(III) complexation with ligand LH1 (**a**) and LH2 (**b**)

anion $L2^{-}$ with Tb(III) ions in a 1:1, 2:1 or 3:1 ratio reproduce this band (at 340 nm) indicating the presence of a coordinated phenolate to the Tb(III) ion.

TEM of Ni-LH1 after terbium addition shows only aggregates of NPs which cannot be further separated, whereas Ni-L2-Tb nanoparticles are well dispersed on the TEM grids (Fig. 7). The colloidal dispersions of Ni-LH2 and Ni-L2-Tb are stable and zeta potential measurements have been performed on the aqueous dispersions. Positive values of zeta potential of 25 ± 20 mV and 30 ± 17 mV have been measured on Ni-LH2 and Ni-L2-Tb respectively in neutral pH dispersion. These values confirm the measurements on commercial Ni nanoparticles without any coating (isoelectric pH of 9–10, $\zeta = 20$ mV at neutral pH) [20]. Thus, the ligand LH2 and Tb complex do not contribute to a drastic change of the surface potential. This presumably precludes the possibility of high surface coverage on the Ni surface, since anionic $L2^{-}$ contribution does not compensate for the positive zeta-potential of Ni at neutral pH.

3 Discussion

3.1 NPs Size, Shape and Interactions

The size, shape and dispersion state of the NPs are deeply influenced by the ligand attached on the surface. A clear contrast is observed between the mono-arm ligand LH1 and the two-arm LH2. Non spherical shapes obtained with LH1 are reminiscent of previous works on shape control [13, 15]. A further control could be achieved by reducing the reaction time and therefore promoting metastable shapes. Nevertheless, the particles display a ferromagnetic behavior due to their size exceeding the limit for the observation of superparamagnetic properties ($\sim$15 nm at room temperature). Magnetic measurements confirm that the blocking temperature is above room temperature for Ni-LH1 (Fig. 8). Ni-LH2 colloids are superparamagnetic with a blocking temperature of 22 K consistent with 4–5 nm Ni nanoparticles (Fig. 7).

In the presence of ligands LH2, the particles display a round shape ($D = 5 \pm 1$ nm from TEM observation) and form very stable colloidal solutions in polar solvents. This could be explained by the pendant OH group of one ligand arm, the other one coordinating the surface. The positive charge of 25 ± 20 mV (as measured by Zeta potential) stabilizes the particles in water for several weeks and opens a way to use Ni for catalytic applications in aqueous media.

3.2 Ligand Configuration on the Nickel Surface

The adsorption of ligands at the surface of transition metal nanoparticles have been investigated for several ligand types like cathecols [21], terpyridines [22], poly-oxometallates [23], and the structure of ligands has been almost resolved for Au clusters [24, 25]. All the spectroscopic experiments presented above confirm the presence of ligands on the surface of Ni, from mass spectrometry, luminescence UV–Vis measurements. The knowledge of ligand conformation at the surface is still challenging and would require a detailed theoretical study since more accurate spectroscopic techniques like NMR are difficult to apply to magnetic materials. Nevertheless, the trend in the stability and the formation of Tb(III) complexes give a solid basis to the following model. Since the fluorescent properties of ligand LH1 or LH2 in the colloidal dispersion

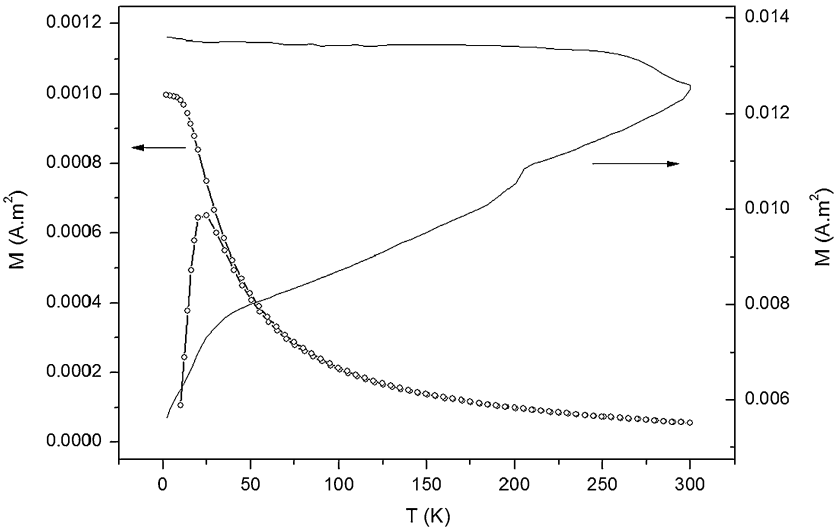

Fig. 8 Zero-field-cooled/field cooled measured under $\mu_0 H = 5.0$ mT on Ni-LH1 (*plain line*) and Ni-LH2 (*line and circles*)

can be observed even after multiple washings, the ligand should bind to the surface through a coordination bond and not weaker Van Der Waals interactions. The analysis of the fluorescence properties suggests that the ligands LH1 and LH2 bind the Ni-surface in the same way, LH1 and $L2^-$ (phenolate) most likely coordinate the Ni surface via the pendant alcohol (Fig. 1).

The structural difference between these two ligands LH1 and LH2 results in a very important effect, when the NPs are reacted with Tb(III) ions. LH1, which possesses only one alcoholic group, is apparently not able to coordinate both the Ni-surface and the Tb(III) ion. Therefore, the addition of Tb(III) displaces the ligand through a competitive coordination and the lanthanide complexes are released from the surface to yield surface free nanoparticles. Due to their size above the superparamagnetic limit the Ni NPs rapidly agglomerate and cannot be further dispersed.

In contrast to LH1, LH2 has shown the ability to coordinate the Tb(III) while remaining adsorbed to the Ni-surface; resulting in the formation of green luminescent NPs dispersion. Raymond and coworkers have shown that, with 2-isophtalamide and salicylamide ligands, stable monoanionic Tb(III) complexes are formed in solution by the *O*,*O*-coordination (acac type) [17]. Since one of the terminal OH group points out of nickel surface, L2 keeps sufficient degrees of freedom to form a *O*,*O*-coordination Tb(III) complex. The ligands appear flexible enough to allow for this rearrangement and partially account for the colloidal stability of the dispersion.

Multidentate coordination has already been observed for Au NPs hybrid systems through molecular or biomolecular surface engineering, leading to sensing devices [26]. In most of the examples reported in the literature, the formation of a complex mediates the interparticle binding of the nanoparticles to affect their plasmonic properties.

In our research, the dispersion of Ni@Tb complex (L2) and precipitation of surface free Ni (LH1) demonstrate the formation of Tb(III) complexes within the ligand shell of the same Ni nanoparticle. An interparticle complex would on the other hand promote the aggregation of a luminescent hybrid in both cases (LH1 and LH2).

The surface cleaning process of catalytic materials such as Ni is an interesting phenomenon and can be linked to the further activity of the catalyst. We have observed that the addition of a lanthanide cation can effectively clean NPs surface, which could find an interesting use since this complexation should not be specific to lanthanides but to most of the transition metals. In this study, the proof of the concept has been achieved with a luminescent complex to probe the mechanism.

4 Conclusion

This synthetic study has established a microwave route towards salicylamide stabilized Ni nanoparticles from an organometallic precursor. Monodentate ligand LH1 stabilizes triangles and rod shape ferromagnetic Ni particles while bidentate LH2 yields superparamagnetic monodisperse spherical Ni nanoparticles. The chemisorption has been followed through the variation of electronic properties of the ligand. Deprotonated $L2^-$ ligand mediates the grafting of luminescent terbium complex on the nickel surface, while LH1 is displaced from Ni surface through Tb(III) addition. Grafting and displacement can be easily followed through the UV–Vis and fluorescence studies. The dispersion of Ni@Tb complex (L2) and precipitation of surface free Ni (LH1) demonstrate the formation of Tb(III) complexes within the ligand shell of the same Ni nanoparticle. This hybrid system is an example of ligand

shell reactivity followed by luminescence measurements and could find applications for monitoring chemical reactions at the surface of Ni nanoparticles.

5 Experimental

5.1 Reagents

$Ni(COD)_2$ (STREM, 98 %), $Tb(NO_3)_3$, $6H_2O$ (STREM, 99.9 %) were used as received. THF has been dried, degassed and stored in a glove box. Ethanol has been distilled twice according to standard procedure.

5.2 Nanoparticles Synthesis

$Ni(COD)_2$ (0.03 mol L^{-1}) is dissolved with the appropriate ligand (LH1 or LH2, 0.03 mol L^{-1}) in anhydrous THF in a glovebox. The solution is then transferred to a special sealed vial for microwave reaction (CEM Discover) and heated at 100 °C (Power 300 W, run time 2 min, hold time 5 min). The same procedure has been repeated for all the ligands. The NPs were then dispersed in ethanol/toluene (1/1), centrifuged and the supernatant was removed. After repeating three times this procedure, the colloids were redispersed in ethanol. $Tb(NO_3)_3{\cdot}6H_2O$ (0.01 mol L^{-1}) was dissolved in ethanol and the colloidal dispersion of Ni-LH was added dropwise and stirred for 5 min. The NPs were then dispersed in ethanol and centrifuge to remove the excess of lanthanide, this procedure was repeated three times and colloids were redispersed in ethanol.

5.3 Mass Spectrometry, Zeta Potential, XRD

ESI mass spectra were recorded on a Q-Tof micro (UK) micromass-waters spectrometer. Zeta potential has been measured on a Zetasizer Nano Z from Malvern instruments. XRD is collected on a Rigaku Ultima IV XRD system. Ni NPs have been drop casted on a glass slide.

5.4 Electron Microscopy

TEM images were obtained from a JEOL-JEM 100SX with 80–100 kV accelerating voltage. High-resolution TEM (HRTEM) images using a JEOL JEM 2100 microscope operating at 200 kV. Samples are prepared by placing a drop of diluted sample on a 400-mesh carbon-coated copper grid.

5.5 Magnetic Measurements

Magnetic properties were measured using a superconducting quantum interference design magnetometer MPMS XL7, in the range of temperature 2–300 K. The temperature-dependent susceptibility was measured using DC procedure. The sample was cooled to 2 K under zero magnetic field, low magnetic field (5.0 mT) was applied and data collected from 2 to 300 K (zero-field cooled). Field cooled measurements were performed from 2 to 300 K with an applied field during the cooling.

References

1. Jia C-J, Schüth F (2011) Phys Chem Chem Phys 13:2457
2. Haslam GE, Chin X-Y, Burstein GT (2011) Phys Chem Chem Phys 13:12968–12974
3. Metin O, Mazumder V, Ozkar S, Sun S (2010) J Am Chem Soc 132:1468
4. Alonso F, Riente P, Yus M (2011) Acc Chem Res 44:379
5. Park J, Kang E, Son SU, Park HM, Lee MK, Kim J, Kim KW, Noh H-J, Park J-H, Bae CJ, Park J-G, Hyeon T (2005) Adv Mater 17:429
6. Ramirez E, Jansat S, Philippot K, Lecante P, Gomez M, Masdeu-Bultó AM, Chaudret B (2004) J Organometal Chem 689:4601–4610
7. Durand J, Teuma E, Gómez M. (2008) Eur J Inorg Chem 23:3577–3586
8. Astruc D, Lu F, Aranzaes JR (2005) Angew Chem Int Ed 44:7852–7872
9. De Caro D, Bradley JS (1997) Langmuir 13:3067
10. Ely TO, Amiens C, Chaudret B, Snoeck E, Verelst M, Respaud M, Broto J-M (1999) Chem Mater 11:526
11. Migowski P, Machado G, Texeira SR, Alves MCM, Morais J, Traverse A, Dupont J (2007) Phys Chem Chem Phys 9:4814
12. Ramírez-Meneses E, Betancourt I, Morales F, Montiel-Palma V, Villanueva-Alvarado CC, Hernández-Rojas ME (2011) J Nanopart Res 13:365
13. Cordente N, Respaud M, Senocq F, Casanove M-J, Amiens C, Chaudret B (2001) Nano Lett 1:565
14. Shviro M, Zitoun D (2012) Nanoscale 4:762
15. Shviro M, Zitoun D (2013) RSC Advances 3:1380
16. Benisvy L, Gamez P, Fu WT, Kooijman H, Spek AL, Meijerink A, Reedijk J (2008) Dalton Trans 24:3147
17. Samuel APS, Xu J, Raymond KN (2009) Inorg Chem 48:687
18. Wanke R, Benisvy L, Kuznetsov ML, Guedes da Silva MFC, Pombeiro AJL (2011) Chem Eur J 17:11882
19. Eckshtain M, Lavi R, Yufit DS, Arora H, Daniel B, Green O, Richman M, Rahimipour S, Gruzman A, Benisvy L (2013) ChemBioChem, submitted
20. Tsai C-J, Chen C-N, Tseng WJ (2011) J Nanoparticle Res 13:6859
21. Yuen AKL, Hutton GA, Masters AF, Maschmeyer T (2012) Dalton Trans 41:2545–2559
22. Winter A, Hager MD, Newkome GR, Schubert US (2011) Adv Mater 23:5728–5748
23. Wang Y, Weinstock IA (2012) Chem Soc Rev 41:7479–7496
24. Daniel M-C, Astruc D (2004) Chem Rev 104:293–346
25. Parker JF, Fields-Zinna CA, Murray RW (2010) Acc Chem Res 43:1289–1296
26. Lim SI, Zhong C-J (2009) Acc Chem Res 42:798–808